Lab on a Chip

RSC Publishing

PAPER

View Article Online
View Journal | View Issue

Single cell detection using 3D magnetic rolled-up structures

Cite this: *Lab Chip*, 2013, **13**, 4225

Tzong-Rong Ger,[a] Hao-Ting Huang,[a] Chen-Yu Huang[a] and Mei-Feng Lai*[ab]

Received 15th June 2013,
Accepted 2nd August 2013

DOI: 10.1039/c3lc50721a

www.rsc.org/loc

A 3D rolled-up structure made of a SiO_2 layer and a fishbone-like magnetic thin film was proposed here as a biosensor. The magnetoresistance (MR) measurement results of the sensor suggest that the presence of the stray field, which is induced by the magnetic nanoparticles, significantly increased the switching field. Comparing the performance of the 2D sensor and 3D sensor designed in this study, the response in switching field variation was 12.14% in the 2D sensor and 62.55% in the 3D sensor. The response in MR ratio variation was 4.55% in the 2D sensor and 82.32% in the 3D sensor. In addition, the design of the 3D sensor structure also helped to attract and trap a single magnetic cell due to its stronger stray field compared with the 2D structure. The 3D magnetic biosensor designed here can provide important information for future biochip research and applications.

Introduction

In biological entities, some minor cells, although extremely low in quantity, are very important such as circulating tumor cells (CTCs), which are the cancer cells that escape into circulating system from the primary tumor and cause cancer metastasis.[1] Therefore, sensing CTCs allows the diagnosis of cancer metastasis at an early stage, and pinpointing these minor cells has become one of the major goals in clinical detection and diagnosis. There is currently extensive research on magnetic carriers as a label and biomedical microchips designs for the sorting and sensing of rare cells.[2–4] The sensing mechanism of a magnetic biosensor that detects magnetically labeled cells mainly lies in the change of the magnetoresistance (MR) of the magnetic sensor's thin films under a magnetic field. The measured signals include the variation of the MR ratio and coercivity caused by the stray field generated by the magnetically labeled specimen.[5,6] However, for the detection of rare cells, the sensitivity of magnetic biosensors is highly demanded because the magnetic signals of the target cells are extremely weak. For this purpose, several types of magnetic biosensors have been reported to address this issue, such as anisotropic magnetoresistance (AMR) sensors,[7,8] giant magnetoresistance (GMR) sensors,[9,10] spin valve sensors[11,12] and Hall effect sensors.[13,14]

In the research of MR detection for magnetic particles, Baselt *et al.* discussed the variation in MR signals of a GMR device caused by the stray field from the magnetic particles.[15] Our previous work used Kerr signals to investigate the change in coercivity of a wave-plate magnetic film structure and MR signals to investigate the MR variation of a wave-like magnetic nanowire caused by a magnetic cell.[16,17] Vavassori *et al.* designed a square-ring structured sensor, and used the domain walls on the corners to attract magnetic particles onto them.[18] Miller *et al.* fabricated a 2D ring-shaped AMR sensing device, and when the magnetic particle was in the center of the ring the stray field from the particle rearranged the spin configuration of the ring into radial direction.[19] Llandro *et al.* proposed a 2D ring-shaped pseudo-spin-valve sensing device to detect the presence of magnetic particles.[20]

Some of the aforementioned studies used 2D ring-shaped sensors of different layer structures for the detection of magnetic particles. The benefit of ring-structured sensors is that they are compatible with the spherical shape of a magnetic particle, so the magnetic stray field emitted from the magnetic particle can be better detected by the sensors. So far, a 3D ring-structured sensor, which is believed to be more sensitive to the magnetic signal of the magnetic particle enclosed, has not been studied yet. In this paper, we propose a 3D rolled-up (3D ring) structure as a magnetic cell sensor that can be used for single cell detection. Fishbone-shaped magnetic films were designed here to actively attract a magnetic cell to the sensor area for magnetoresistance measurement.

Experimental

I. Design and fabrication

The rolled-up structure with fishbone-like $Ni_{80}Fe_{20}$ magnetic thin films was fabricated using standard electron beam (e-beam) lithography, e-beam evaporation, a lift-off process, and

[a]*Department of Power Mechanical Engineering, National Tsing Hua University, Hsinchu 300, Taiwan*
[b]*Institute of NanoEngineering and MicroSystems, National Tsing Hua University, Hsinchu 300, Taiwan. E-mail: mflai@mx.nthu.edu.tw*

a wet-etching process.[21] A commercial scanning electron microscope (SEM) was modified for e-beam lithography. First, through e-beam lithography, fishbone-shaped patterns were created onto a SiO_2-coated (100 nm thick) silicon substrate that was spin-coated with e-beam resist polymethyl methacrylate (PMMA). Later, the sample was developed in a 3 : 1 mixture of 2-propanol and methyl isobutyl ketone, and then the fishbone-shaped trenches formed in PMMA. We used the e-beam evaporation system to deposit 10 nm thick Cr as the adhesive layer, 90 nm thick $Ni_{80}Fe_{20}$ as the sensing layer, and 10 nm thick Cr as the capping layer in sequence. The temperature of the substrate was kept at room temperature and no external field was applied during the deposition. After the lift-off process in acetone, all remaining resist was removed and the fishbone-shaped magnetic thin films were obtained on the substrate. Subsequently, the same e-beam lithography and e-beam evaporation processes were performed again to make the gold electrodes for MR measurement. To obtain the 3D rolled-up structure, we created a SiO_2 opening using buffered oxide etchant (BOE). Subsequently, the substrate was immersed in tetramethylammonium hydroxide (TMAH) for an hour to remove the silicon under the structure, and the rolled-up structure was then obtained due to the different thermal expansion coefficients of the film materials.[22] Finally, the substrate was washed with deionized water until the pH was neutral and it was then sterilized using 70% ethanol. To avoid deformation or collapse of the structure, the solvents were removed using a heat-drying process.

II. Magnetic cell preparation and culture

NPC-TW01 cells that are a type of adherent cells were cultured in Dulbecco's modified eagle's medium (DMEM) containing 1% penicillin and 10% fetal calf serum at 37 °C in a 5% CO_2 environment. Before the sensing experiment, the cells were co-cultured for 24 h with a diluted ferrofluid (EMG 705, Ferrotec) at a concentration of 1 μg ml^{-1}. The ferrofluid consisted of Fe_3O_4 magnetic nanoparticles, whose average diameter was 10 nm. During co-culture, the magnetic nanoparticles entered the cells so the cells were magnetically labeled. Subsequently, the magnetically labeled cells were washed 3 times by centrifugation at 1500 rpm for 5 min and the solution was replaced by fresh PBS to remove residual magnetic nanoparticles. Finally, the cells were concentrated by applying a magnetic field gradient using a permanent magnet (NdFeB) that was placed on the outer wall of the centrifuge tube, and the magnetically labeled cells collected were then put in a clean culture medium. Before we used SEM to observe the morphology of the 3D rolled-up structure that trapped a single cell, the sample was washed with phosphate buffer solution (PBS) and then fixed with 3.7% formaldehyde for 30 min. The sample was then dehydrated by a series of graded ethanol solutions. After being dried at room temperature, the sample was coated with a very thin Cr layer before being examined by SEM.

III. Magnetophoresis test

Magnetophoresis was used in our study to estimate the number of the magnetic nanoparticles in the NPC-TW01 cells.[17,23,24] A permanent magnet was used to provide the field gradient, which led to a cell velocity distribution. The balance between the viscous force $F_{vis} = 6\pi\eta Rv$ given by Stokes' law and the magnetic force $F_m = m_{bead}dB/dx$ exerted on a cell with magnetic moment m_{bead} under a magnetic field gradient dB/dx (12 mT mm^{-1}) was used to estimate the number of magnetic nanoparticles inside each cell

$$6\pi\eta Rv = m_{bead}dB/dx \quad (1)$$

where $\eta = 0.013$ Pa s is the viscosity of the medium at 37 °C,[25] v is the cell velocity, and R is the average radius of each NPC-TW01 cell. The total magnetic moment of the magnetic nanoparticles inside a cell can be expressed as $m_{bead} = NcM_s\pi D^3/6$,[26–28] where N is the total number of magnetic nanoparticles per cell, c is the ratio of the net magnetization of magnetic nanoparticles to their saturation magnetization M_s, and D is the average diameter of each magnetic nanoparticle. Substituting m_{bead} into eqn (1), the number of magnetic nanoparticles can be expressed as:

$$N = (36\eta Rv)/(cM_sD^3dB/dx) \quad (2)$$

According to the experimental result obtained in previous literature,[29,30] the parameter c can be set as 0.8 and $M_s = 4.84 \times 10^5$ A m^{-1}. Therefore, using eqn (2), the number N of magnetic nanoparticles per cell can be estimated.

IV. Experimental procedure

The 3D rolled-up structure was pre-magnetized in Hx direction with an applied magnetic field of 2000 Oe before sensing cells. The magnetic force that was generated by the magnetic field gradient of the fishbone-shaped magnetic films then attracted the magnetic cell to the sensor structure for MR measurement. In the sensing experiment, we measured the MR curves for 2D structure (without rolling up) and 3D structure (rolling up) when the fields H_x and H_y were applied in the x and y directions, respectively (see Fig. 1), to derive the switching field and MR ratio. By comparing the signals obtained before and

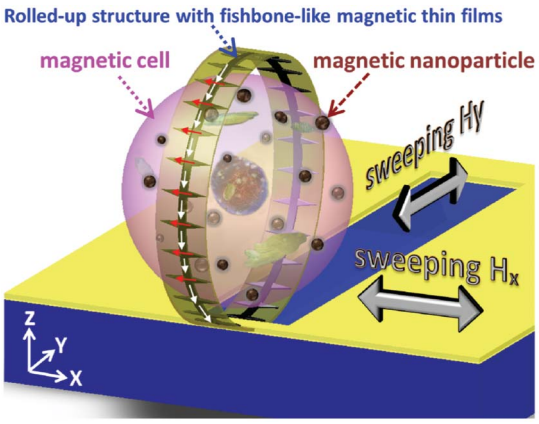

Fig. 1 Illustration of the rolled-up structure with fishbone-like magnetic thin films where a cell labeled with magnetic nanoparticles was trapped inside. Magnetic fields H_x and H_y were applied in the x and y directions, respectively, for the measurement of magnetoresistance.

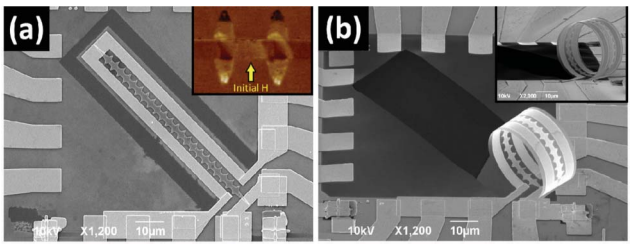

Fig. 2 SEM images of (a) planar and (b) rolled-up fishbone-like magnetic thin film. The inset in (a) is the MFM image of the remanent state of the fishbone magnetic thin films after it was magnetized by an initial magnetic field *H* (2000 Oe). The inset in (b) is the tilted view SEM image.

after the single cell was attached, we can determine the sensitivity of the 2D and 3D cell sensors.

Results and discussion

Fig. 2(a) represents the SEM image of the fishbone-like magnetic film with a total length of 80 μm before being released from the Si substrate. In our fishbone-like structure, the magnetic thin film is cross-structured. When a magnetic field was applied parallel to the tapered film, a magnetization configuration with lowest energy occurred. The inset of Fig. 2(a) shows the magnetic force microscope (MFM) image of the fishbone-like magnetic thin film. From the MFM image it can be observed that the tapered film exhibits a magnetic single domain configuration, which produces the largest stray field for attracting cells in a solution. Fig. 2(b) shows the magnetic film released from the substrate, where the film has rolled up to form a 3D structure with a diameter of 25 μm, a size that is suitable for single cell detection. The cell velocity distribution of magnetically labeled NPC-TW01 cells obtained from magnetophoresis experiment is shown in Fig. 3(a). The average velocity 6.17 $\pm$ 2.78 μm s^{-1} was derived after measuring the individual velocities of 810 magnetic cells. The average diameter of the NPC-TW01 cells was 14.4 μm, and the amount of magnetic nanoparticles was estimated to be $(4.474 \pm 2.013) \times 10^6$ per cell. Fig. 3(b) shows a magnetically labeled NPC-TW01 cell after Prussian blue staining and nuclear fast red counterstaining. It can be observed that after 24 h co-culture of NPC-TW01 cells and ferrofluid, the magnetic nanoparticles entered the cytoplasm by the process of endocytosis [see the arrow in Fig. 3(b)].

The magnetic film was designed to be fishbone-shaped with sharpened protrusions such that the large magnetic shape anisotropy caused by the sharp ends can favor the formation of magnetic single-domain state, which generated a magnetic field gradient to attract the magnetic cell to the sensor structure for MR measurement. Fig. 4 represents the sequential optical microscope (OM) images of a single magnetic cell when the latter was gradually attracted to the 3D rolled-up sensor structure. After 50 s the target cell was attracted to the 3D rolled-up structure, as we can see clearly

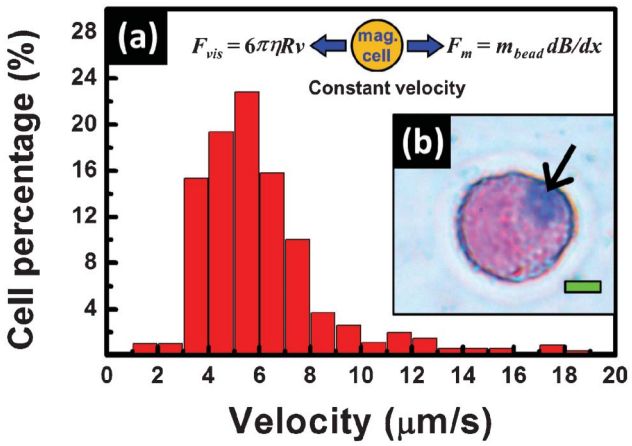

Fig. 3 (a) The velocity distribution of NPC-TW01 cells obtained using magnetophoresis after 24 h of cultivation in ferrofluid with concentration of 1 μg ml^{-1}. The total number of the cells counted was 810, and the average cell velocity was calculated to be 6.17 $\pm$ 2.78 μm s^{-1}. (b) OM image of the magnetic cell stained with Prussian blue and nuclear fast red. The distribution of magnetic nanoparticles in the cytoplasm of the NPC-TW01 cell is indicated by the arrow. The scale bar indicates 4 μm.

from the enlarged images in Fig. 4(f) and 4(g) when the focus was on the 3D sensor structure and on the cell, respectively. In a non-uniform field created by the magnetic 3D ring structure, the magnetic cell experiences a force, F_{mag}, that tends to pull the magnetic cell toward the maximum field gradient. When the viscous force from the medium solution and the magnetic force exerted on the magnetic cell balance out, the cell moves at a constant velocity *v*. According to our observation using optical microscopy, the cell moved at a constant velocity in the medium under the attraction of the magnetic 3D ring structure, so the magnetic attraction force can be estimated from the viscous force using Stokes' equation $F = 6\pi\eta KRv$, where η = 0.013 Pa s is the viscosity of the medium at 37 °C and

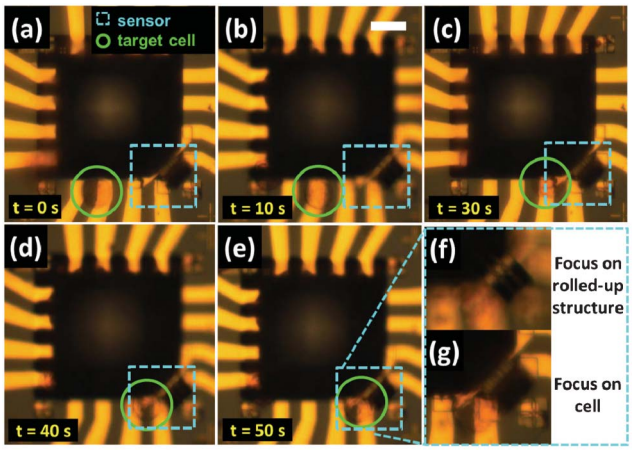

Fig. 4 (a)–(e) Sequential OM images of a single target cell being attracted to the 3D rolled-up magnetic structure; (f),(g) OM images with the focus on the sensor structure and the cell, respectively. The dashed circle indicates the 3D rolled-up magnetic sensor and the open circle indicates the target cell.

K is a factor that varies between 1.0 when the cell is far from the plane wall and 1.7 when the cell is near the plane wall;[31] R is the average radius of each cell and v is the speed of the cell. The magnetic attraction force was estimated to be 3 pN, in the same order as the results given in the previous literature.[32–34] Assuming that the magnetic field uniformly saturated each magnetic nanoparticle, and that the magnetized nanoparticles experienced an equal magnetic field gradient, the total magnetic force on the cell can be written as $F_{mag} = m_{bead}\nabla B$. The total magnetic moment of the magnetic nanoparticles inside a cell $m_{bead} = NcM_s\pi D^3/6$,[26–28] where N is the number of magnetic nanoparticles per cell that are magnetized, c is the ratio of the net magnetization of magnetic nanoparticles to their saturation magnetization M_s, and D is the average diameter of each magnetic nanoparticle. From the discussion above, the magnetic attraction force F_{mag} was estimated to be 3 pN, so the magnetic field gradient caused by the magnetic 3D ring structure can be estimated to be 0.033 Gauss μm^{-1}.

Fig. 5(a) represents the fluorescent OM image of a cell with GFP expression, showing that the cell was totally trapped inside the 3D rolled-up magnetic structure. The GFP expression indicated that the cell was alive during measurement. Fig. 5(b) shows the SEM image of a cell inside the 3D structure. The slight deformation of the 3D rolled-up structure was caused by the fixation, dehydration and drying procedures during the sample preparation for SEM imaging. The success rate for cell trapping in a static solution is determined by the concentration of cells in the cell solution, the density of the sensors, the sediment rate of the cells, and so on. On average, a single cell could be attracted by the stray field of the magnetic 3D sensor structure within a distance of about 60 μm in our experiment. That means if at least one cell lies within the upper hemisphere of radius 60 μm above the sensor, the sensor can trap a cell. Therefore, the cell concentration should be at least 2.2×10^6 cells ml^{-1} to assure 100% cell trapping. At a lower cell concentration, the success rate for cell trapping might be lower accordingly. However, the above estimation is made in a static solution, however if it is in a dynamic solution with slow flow velocity, the flow of the cells can increase the probability of cell trapping by the 3D sensor.

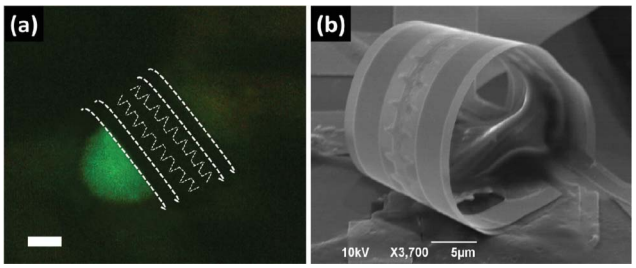

Fig. 5 (a) Fluorescent OM image of a cell with GFP expression inside a 3D rolled-up magnetic structure, whose contour is shown by the dashed lines. The GFP expression indicated that the cell was alive during measurement. (b) SEM image of a single cell, which was dehydrated and dried, trapped in the 3D magnetic sensor.

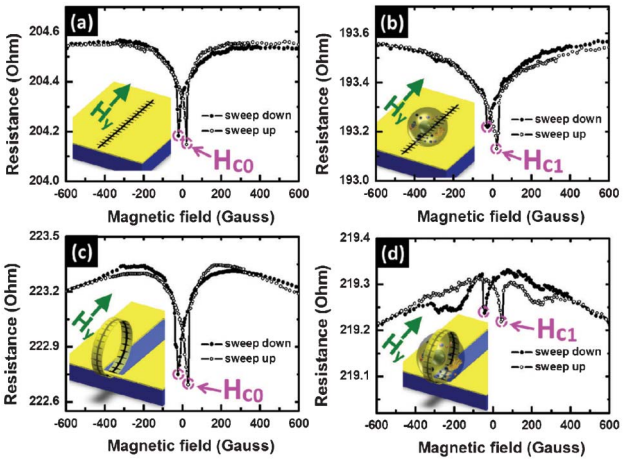

Fig. 6 (a),(b) MR curves of the 2D planar sensor without and with magnetic cell attached; (c),(d) MR curves of the 3D rolled-up sensor without and with single magnetic cell attached. The magnetic field swept in the y direction. The dashed circles indicate the switching field of the sensors where H_{c0} indicates the switching field when no magnetic cell was attached on the sensor and H_{c1} indicates the switching field when a single magnetic cell was attached.

Fig. 6 represents the MR curves measured when the field swept along the H_y direction. Fig. 6(a) is the MR curve of the 2D planar fishbone magnetic film before a magnetic cell was attached, where the dashed circles indicate the switching field H_{c0} of the magnetization process, which in this case is 20.75 Gauss as an average of the switching fields in the sweep-up and sweep-down processes. The subscript 0 in H_{c0} indicates that no cell was attached. The MR ratio is defined as $(R_{max} - R_{min})/R_{max}$, which is in this case 0.194%. When a magnetic cell was attached on the 2D planar fishbone magnetic film (see Fig. 6(b)), the switching field H_{c1} became 23.1 Gauss. The subscript 1 in H_{c1} indicates that a cell was attached. Comparing the MR curves of the 2D sensor before and after the attachment of a cell, the switching field changed from 20.75 Gauss to 23.1 Gauss, and the MR ratio changed from 0.194% to 0.193%. The variation was not large. In contrast, for the 3D rolled-up structure, the variations of switching fields and MR ratios between pre-attachment and post-attachment of a magnetic cell were relatively remarkable. Fig. 6(c) shows the MR curves of 3D rolled-up magnetic structure before a magnetic cell was attached. The switching field H_{c0} and the MR ratio were 26.7 Gauss and 0.279%, respectively. When a magnetic cell was attached (see Fig. 6(d)), the switching field H_{c1} and the MR ratio became 43.4 Gauss and 0.05%, respectively. The increase of the switching field for both 2D and 3D structures after the attachment of a magnetic cell is believed to be caused by the influence of the stray field of the magnetic cell on the magnetic sensor structure. As we can see from Fig. 7(a) and 7(b), the stray field generated by the magnetic cell when a magnetic field was applied was opposed to the direction of the applied field on the sensor region, so it required larger field to complete the switching process. For the 3D structure (see Fig. 7(b)), the influence of the stray field on the switching field was much larger than the 2D structure (see

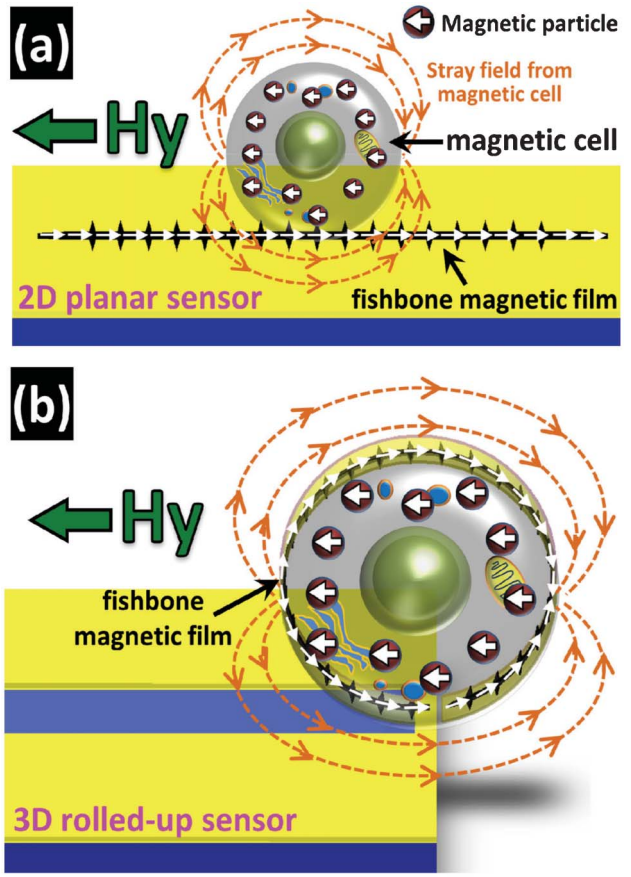

Fig. 7 Illustrations of the stray field generated by the magnetic cell influence the (a) 2D planar sensor region and (b) 3D rolled-up sensor region when a magnetic field (H) was applied was opposed to the direction of the applied field.

Fig. 7(a)) because in the 3D structure the magnetic cell was enclosed by the fishbone magnetic film.

Fig. 8 represents the MR curves measured when the field was swept along the H_x direction. Comparing the two MR curves in Fig. 8(a) and 8(b), which correspond to 2D planar magnetic film structures with and without the attachment of a magnetic cell, respectively, the magnetic switching field changes from H_{c0} = 44 Gauss in Fig. 8(a) to H_{c1} = 52.9 Gauss in Fig. 8(b). Comparing the two MR curves in Fig. 8(c) and 8(d), which correspond to 3D rolled-up magnetic film structures with and without the attachment of a magnetic cell, respectively, the magnetic switching field changes from H_{c0} = 101.9 Gauss in Fig. 8(c) to H_{c1} = 144.1 Gauss in Fig. 8(d). Fig. 8 shows the comparison of the response to the attachment of a magnetic cell between 2D and 3D magnetic biosensors. $\Delta H_c/H_{c0}$ in Fig. 9(a) represents the switching field variation ($\Delta H_c \equiv H_{c1} - H_{c0}$) normalized by the initial switching field H_{c0}; $|\Delta MR_{ratio}|/MR_{ratio0}$ in Fig. 9(b) represents the MR ratio variation ($|\Delta MR_{ratio}| \equiv |MR_{ratio1} - MR_{ratio0}|$) normalized by the initial MR ratio MR_{ratio0}. The subscripts 0 and 1 represent the pre-attachment and post-attachment of a magnetic cell, respectively. It can be clearly observed that the response to the attachment of a magnetic cell for the 3D magnetic biosensor

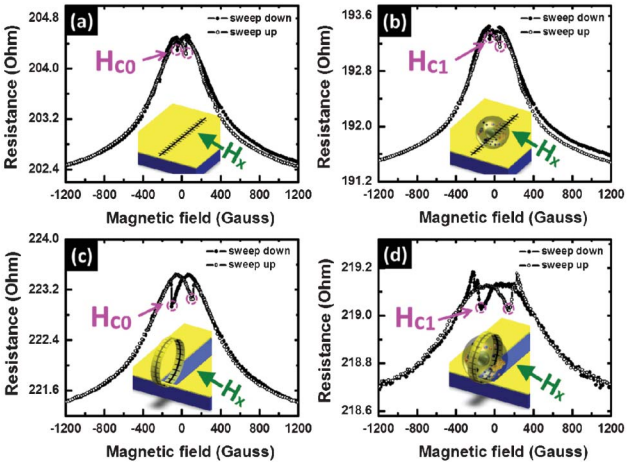

Fig. 8 (a),(b) MR curves of the 2D planar sensor without and with magnetic cell attached; (c),(d) MR curves of the 3D rolled-up sensor without and with single magnetic cell attached. The magnetic field swept in the x direction. The dashed circles indicate the switching field of the sensors where H_{c0} indicates the switching field when no magnetic cell was attached on the sensor and H_{c1} indicates the switching field when a single magnetic cell was attached.

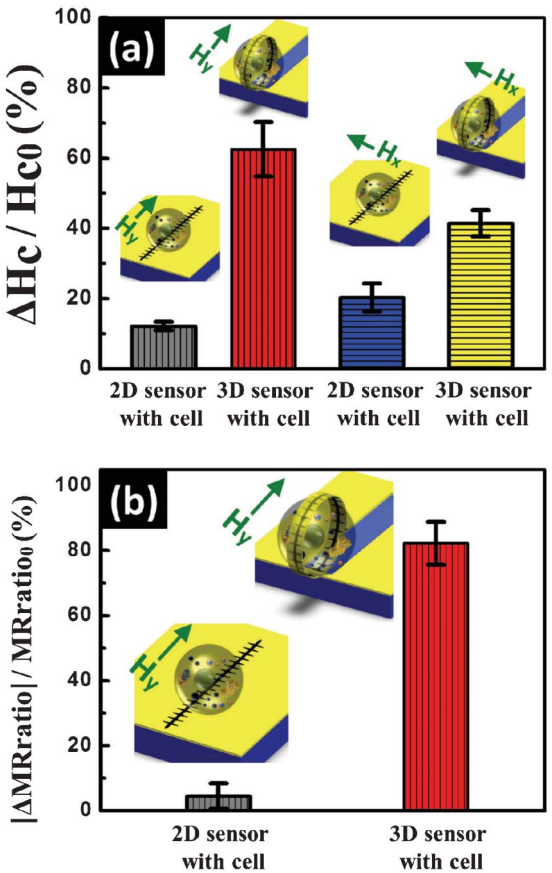

Fig. 9 (a) Reduced variation of the switching field of 2D and 3D magnetic cell sensors when a single magnetic cell was attached. $\Delta H_c \equiv H_{c1} - H_{c0}$. (b) Reduced variation of the MR ratio of 2D and 3D magnetic cell sensors when a single magnetic cell was attached. $\Delta MR_{ratio} \equiv MR_{ratio1} - MR_{ratio0}$ where MR_{ratio1} represents the MR ratio when a single magnetic cell was attached on the sensor and MR_{ratio0} represents the MR ratio when no magnetic cell was attached.

was much larger than that for the 2D magnetic biosensor owing to the reason mentioned in the last paragraph. It also means that the 3D magnetic biosensor has much a higher sensitivity than the 2D one. Planar magnetic thin film ring[35] is an interesting physical system that is suitable for the studies of domain wall nucleation, annihilation and propagation, and it has attracted much attention since the last decade. For the 3D ring structure proposed in this study, when a magnetic field is applied radially, the magnetic field is out-of-the-plane at the two ends of the 3D ring along the field. Therefore, this proposed 3D ring structure can provide another interesting physical system for investigating domain wall nucleation, annihilation, propagation, and so on.

Conclusions

In summary, the proposed 3D magnetic biosensor had much higher sensitivity than the 2D magnetic biosensor as a result of its rolled-up structure which can enclose the magnetic cell during measurement to enhance the signal. The rolled-up structure of the sensor can also ''smartly'' attract the magnetic cell to the sensor area for active detection, so it is very useful for detecting very small amounts of cells that are generally hard to detect. This 3D magnetic biosensor has the potential to be integrated on a microfluidic channel for cell detection and cell counting, which will be studied in our future work. The 3D magnetic biosensor designed here can provide important information for future biochip research and applications.

Acknowledgements

This work was supported partly by the ROC National Science Council Grant Numbers NSC 99-2112-M-007-016-MY3, NSC 99-2112-M-007-015-MY3, NSC 102-2112-M-007-006-MY3 and NSC 102-2112-M-007-012 -MY3.

References

1 P. Paterlini-Brechot and N. L. Benali, *Cancer Lett.*, 2007, **253**, 180–204.
2 E. I. Galanzha, E. V. Shashkov, T. Kelly, J. W. Kim, L. Yang and V. P. Zharov, *Nat. Nanotechnol.*, 2009, **4**, 855–860.
3 S. Nagrath, L. V. Sequist, S. Maheswaran, D. W. Bell, D. Irimia, L. Ulkus, M. R. Smith, E. L. Kwak, S. Digumarthy and A. Muzikansky, *Nature*, 2007, **450**, 1235–1239.
4 A. A. Adams, P. I. Okagbare, J. Feng, M. L. Hupert, D. Patterson, J. Göttert, R. L. McCarley, D. Nikitopoulos, M. C. Murphy and S. A. Soper, *J. Am. Chem. Soc.*, 2008, **130**, 8633–8641.
5 J. Llandro, J. Palfreyman, A. Ionescu and C. H. W. Barnes, *Med. Biol. Eng. Comput.*, 2010, **48**, 977–998.
6 D. L. Graham, H. A. Ferreira and P. P. Freitas, *Trends Biotechnol.*, 2004, **22**, 455–462.
7 M. Miller, G. Prinz, S. F. Cheng and S. Bounnak, *Appl. Phys. Lett.*, 2002, **81**, 2211–2213.
8 Z. Jiang, J. Llandro, T. Mitrelias and J. Bland, *J. Appl. Phys.*, 2006, **99**, 08S105.
9 R. S. Gaster, D. A. Hall, C. H. Nielsen, S. J. Osterfeld, H. Yu, K. E. Mach, R. J. Wilson, B. Murmann, J. C. Liao and S. S. Gambhir, *Nat. Med.*, 2009, **15**, 1327–1332.
10 J. Rife, M. Miller, P. Sheehan, C. Tamanaha, M. Tondra and L. Whitman, *Sens. Actuators, A*, 2003, **107**, 209–218.
11 H. Ferreira, D. Graham, P. Freitas and J. Cabral, *J. Appl. Phys.*, 2003, **93**, 7281–7286.
12 G. Li, V. Joshi, R. L. White, S. X. Wang, J. T. Kemp, C. Webb, R. W. Davis and S. Sun, *J. Appl. Phys.*, 2003, **93**, 7557–7559.
13 G. Landry, M. Miller, B. Bennett, M. Johnson and V. Smolyaninova, *Appl. Phys. Lett.*, 2004, **85**, 4693–4695.
14 P. Manandhar, K. S. Chen, K. Aledealat, G. Mihajlović, C. S. Yun, M. Field, G. J. Sullivan, G. F. Strouse, P. B. Chase and S. von Molnár, *Nanotechnology*, 2009, **20**, 355501.
15 D. R. Baselt, G. U. Lee, M. Natesan, S. W. Metzger, P. E. Sheehan and R. J. Colton, *Biosens. Bioelectron.*, 1998, **13**, 731–739.
16 T. R. Ger, Y. R. Xu, H. T. Huang and Z. H. Wei, *J. Appl. Phys.*, 2012, **111**, 07E506.
17 H. T. Huang, T. R. Ger, Y. H. Lin and Z. H. Wei, *Lab Chip*, 2013, **13**, 3098–3104.
18 P. Vavassori, V. Metlushko, B. Ilic, M. Gobbi, M. Donolato, M. Cantoni and R. Bertacco, *Appl. Phys. Lett.*, 2008, **93**, 203502.
19 M. Miller, G. Prinz, S. F. Cheng and S. Bounnak, *Appl. Phys. Lett.*, 2002, **81**, 2211–2213.
20 J. Llandro, T. Hayward, D. Morecroft, J. Bland, F. Castano, I. Colin and C. Ross, *Appl. Phys. Lett.*, 2007, **91**, 203904.
21 T. R. Ger, H. T. Huang, W. Y. Chen and M. F. Lai, *Lab Chip*, 2013, **13**, 2364–2369.
22 M. Ataka, A. Omodaka, N. Takeshima and H. Fujita, *J. Microelectromech. Syst.*, 1993, **2**, 146–150.
23 A. K. A. Silva, C. Wilhelm, J. K. Tabi, N. Luciani and F. Gazeau, *Pharm. Res.*, 2012, **29**, 1392–1403.
24 M. F. Lai, C. Y. Chen, C. P. Lee, H. T. Huang, T. R. Ger and Z. H. Wei, *Appl. Phys. Lett.*, 2010, **96**, 183701.
25 W. Yi, Y. Sun, X. Wei, C. Gu, X. Dong, X. Kang, S. Guo and K. Dou, *Mol. Cell. Biochem.*, 2010, **341**, 9–16.
26 T. Ozkaya, M. S. Toprak, A. Baykal, H. Kavas, Y. Köseoğlu and B. Aktaş, *J. Alloys Compd.*, 2009, **472**, 18–23.
27 D. E. Markov, H. Boeve, B. Gleich, J. Borgert, A. Antonelli, C. Sfara and M. Magnani, *Phys. Med. Biol.*, 2010, **55**, 6461–6473.
28 I. Slabu, G. Guntherodt, T. Schmitz-Rode, M. Hodenius, N. Kramer, H. Donker, G. A. Krombach, J. Otto, U. Klinge and M. Baumann, *Curr. Pharm. Biotechnol.*, 2012, **13**, 545–51.
29 G. F. Goya, T. S. Berquó, F. C. Fonseca and M. P. Morales, *J. Appl. Phys.*, 2003, **94**, 3520.
30 Y. Yang, R. M. Erb, B. J. Wiley, S. Zauscher and B. B. Yellen, *Nano Lett.*, 2011, **11**, 1681–1684.
31 A. J. Goldman, R. G. Cox and H. Brenner, *Chem. Eng. Sci.*, 1967, **22**, 653–660.
32 J. H. Koschwanez, R. H. Carlson and D. R. Meldrum, *Rev. Sci. Instrum.*, 2007, **78**, 044301.
33 S. Anandakumar, V. S. Rani, S. Oh, B. L. Sinha, M. Takahashi and C. Kim, *Biosens. Bioelectron.*, 2010, **26**, 1755–1758.
34 P. Tierno, S. V. Reddy, J. Yuan, T. H. Johansen and T. M. Fischer, *J. Phys. Chem. B*, 2007, **111**, 13479–13482.
35 M. F. Lai, Z. H. Wei, C. R. Chang, J. C. Wu, J. H. Kuo and J. Y. Lai, *Phys. Rev. B: Condens. Matter*, 2003, **67**, 104419.

